



(22) Date de dépôt/Filing Date: 2008/03/10
(41) Mise à la disp. pub./Open to Public Insp.: 2009/05/15
(30) Priorité/Priority: 2007/11/15 (US60/988,289)

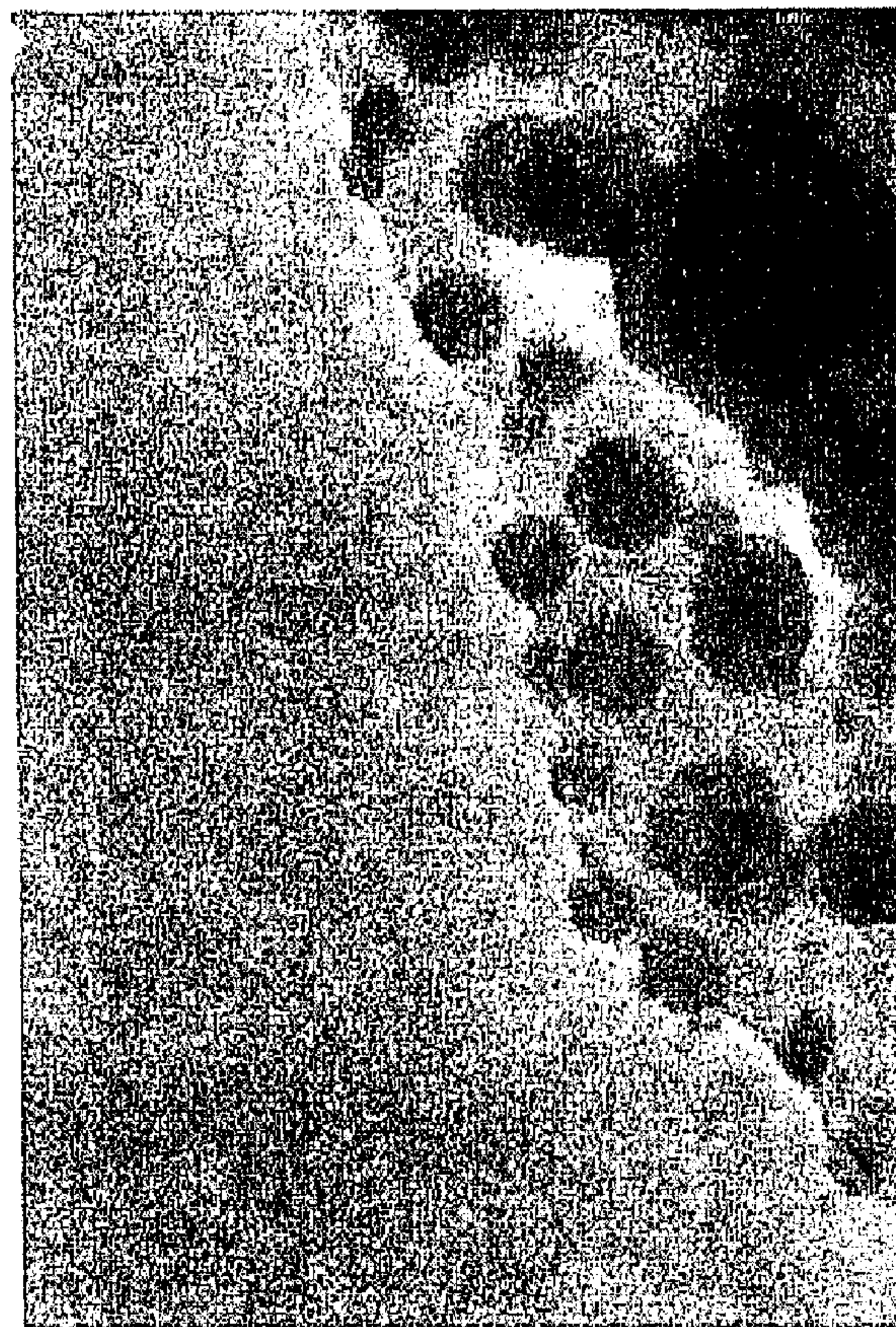
(51) Cl.Int./Int.Cl. *C01B 39/02* (2006.01),
A61K 33/38 (2006.01), *A61P 31/00* (2006.01),
C01B 23/00 (2006.01), *C01G 3/00* (2006.01),
C01G 5/00 (2006.01), *C01G 53/00* (2006.01),
C01G 55/00 (2006.01), *C01G 7/00* (2006.01)

(71) Demandeur/Applicant:
THE GOVERNORS OF THE UNIVERSITY OF
ALBERTA, CA

(72) Inventeur/Inventor:
KUZNICKI, STEVEN J., CA

(74) Agent: BENNETT JONES LLP

(54) Titre : NANOPPOINTS METALLIQUES A SUPPORT DE ZEOLITE
(54) Title: ZEOLITE SUPPORTED METALLIC NANODOTS



20 nm

(57) Abrégé/Abstract:

A metal nanodot material is formed by ion-exchange with an ETS zeolite, followed by activation to form metallic nanodots. The nanodot may be formed from silver, nickel, copper, gold or a platinum group metal.

5

ABSTRACT

A metal nanodot material is formed by ion-exchange with an ETS zeolite, followed by activation to form metallic nanodots. The nanodot may be formed from silver, nickel, copper, gold or a platinum group metal.

5

ZEOLITE SUPPORTED METALLIC NANODOTS**Field of the Invention**

The present invention relates to metal nanodots formed on ETS materials and to methods
10 of gas adsorption using metal nanodots formed on ETS materials.

Background

Metal nanoparticles and nanowires are the subject of current research efforts motivated by
their high potential utility derived from nanoscale induced optical, electrical and chemical
properties.

15 A wide range of techniques has been reported to synthesize metal nanoparticles including
numerous high vacuum approaches as well as a range of photochemical [1–3] and thermal
methods [4–7]. A technique that is just beginning to gain attention is the potential use of
zeolite surfaces to induce the growth of metal nanostructures [8–10]. With many of their
properties manifested on a nano- and subnano- dimensional scale, molecular sieves would
20 appear to be excellent candidates to be in the vanguard of such nanofabrication efforts [11].

Unfortunately, current techniques for generation of metal nanoparticles, such as nanosilver
generation, are expensive and cumbersome [14]. Subnanometer silver ensembles can be
induced to form within zeolite cavities under certain conditions [15–18], and much larger
configurations often form on zeolite surfaces under reductive atmospheres. While metals
25 readily congregate on zeolite surfaces, achieving stable, zeolite supported metal nanoscale
structures has proved difficult because of the high metal mobility generally seen on zeolite

5 surfaces. Typically, upon reduction, metals ion-exchanged into zeolite crystals diffuse to the crystal surface and rapidly coalesce into micron-scale agglomerates [19, 20]. Because of the low surface to volume ratio of these agglomerates (compared to nanometal ensembles), they generally behave like bulk metals, not displaying the novel properties anticipated for nanoparticulates.

10 Nanoparticulate silver has many potential uses. Many useful properties might be expected if inexpensive nanostructured silver materials were readily available. Silver is a well-known antimicrobial agent and nanoscale silver is finding increasing usage in medical devices, bandages and related medical applications [12, 13]. Current methods to generate nanosilver center on complex techniques such as surface sputtering. Research level work in biomedical
15 engineering implants is showing promise in nanosilver bone cements where nanoparticle size control ranges from 5 nm to 50 nm [21].

Powerful surface plasmon absorption of nanoparticulate silver makes them particularly useful in applications such as biosensors, for example. Silver nanodots may be photo-fluorescence markers, which make them useful for a number of medical and similar
20 applications. They are environmentally and biologically benign. Other exemplary silver nanodot applications include smart windows, rewritable electronic paper, electronic panel displays, memory components, and others.

A wide range of techniques has been reported to synthesize metal nanodots. Silver nanodots and their formation have recently been discussed by Metraux and Mirkin, 2005 [14].
25 Traditional methods for the production of silver nanodots require use of potentially harmful

5 chemicals such as hydrazine, sodium borohydride and dimethyl formamide ("DMF"). These chemicals pose handling, storage, and transportation risks that add substantial cost and difficulty to the production of silver nanodots. A highly trained production workforce is required, along with costly production facilities outfitted for use with these potentially harmful chemicals.

10 Another disadvantage of known methods for producing silver nanodots relates to the time and heat required for their production. Known methods of production utilize generally slow kinetics, with the result that reactions take a long period of time. The length of time required may be shortened by some amount by applying heat, but this adds energy costs, equipment needs, and otherwise complicates the process. Known methods generally require reaction for
15 20 or more hours at elevated temperatures of 60° to 80°C, for example. The relatively slow kinetics of known reactions also results in an undesirably large particle size distribution and relatively low conversion. The multiple stages of production, long reaction times at elevated temperatures, relatively low conversion, and high particle size distribution of known methods make them costly and cumbersome, particularly when practiced on a commercial scale.

20 While silver ensembles are well known to form within zeolite cavities under certain conditions, and much larger configurations often form freely on zeolite surfaces, nanodots have not been known to form on zeolite surfaces in concentrations higher than trace levels.

These and other problems with presently known methods for making silver nanodots are exacerbated by the relatively unstable nature of the nanodots. Using presently known

5 methods, silver nanodots produced have only a short shelf life since they tend to quickly agglomerate.

Therefore, there is a need in the art for a convenient and inexpensive method of forming metal nanodots, such as silver nanodots, which mitigates the difficulties of the prior art.

Summary Of The Invention

10 In one aspect, the invention comprises a method of forming metal nanodots on an ETS zeolite surface. Metal ion-exchange with the ETS zeolite is followed by activating at moderate temperatures. In one embodiment, the ETS zeolite comprises ETS-10 and materials which are isostructural with ETS-10. In another aspect, the invention comprises a plurality of metal nanodots, formed by ion-exchange and subsequent activation on ETS-10. In one
15 embodiment, the metal may comprise a transition or noble metal, for example, copper, nickel, palladium or silver.

In one embodiment, silver is a preferred metal. In one embodiment, silver nanodots may form having diameters less than about 100 nm, for example, less than about 50 nm, 30 nm, 20 nm, or 10 nm. In one embodiment, the nanodots are in the order of about 5 to about 15 nm,
20 with a mean of about 10 nm, forming under a wide range of conditions on ETS zeolite surfaces.

The present invention is distinctly different from the well established science of growing metal nanodots or nanowires within a zeolite cage framework, thus producing nanostructures

5 inside the material. In the present invention, unlike in the prior art, the metallic nanodots are surface-accessible on the ETS zeolite support.

Nanostructured silver materials produced in accordance with the present invention may have many useful properties. In one aspect, the invention may comprise the use of nanodots of silver to selectively adsorb rare gases, such as argon, krypton, xenon, or radon. In one
10 embodiment, argon may be separated from an oxygen stream or xenon may be separated from air, or from a gas stream comprising nitrogen and oxygen.

In another aspect, the invention may comprise the use of nanodots of silver as an antibacterial or antifungal agent.

Therefore, in one aspect, the invention may comprise a method of forming a metal
15 nanoparticulate material, comprising the steps of:

- (a) performing ion-exchange with a solution of the metal ions and an ETS zeolite; and
- (b) activating the ion-exchanged ETS zeolite.

In another aspect, the invention may comprise an ETS-10 supported metal nanoparticulate material, comprising surface-accessible particles of metal, having a substantially uniform
20 particle size less than about 100 nm, for example, less than about 50 nm, 30 nm, or 20 nm. In one embodiment, the material may comprise metal nanodots having a diameter in the range of about 5 nm to about 15 nm, and on average about 10 nm.

Brief Description Of The Drawings

5 In the drawings, like elements are assigned like reference numerals. The drawings are not necessarily to scale, with the emphasis instead placed upon the principles of the present invention. Additionally, each of the embodiments depicted are but one of a number of possible arrangements utilizing the fundamental concepts of the present invention. The drawings are briefly described as follows:

10 Figure 1 shows a TEM image of silver nanoparticles on Ag-ETS-10.

Figure 2 is a graph showing xenon adsorption isotherms at 25°C for raw (NA-ETS-10) and modified (Ag-ETS-10) samples.

Figure 3(a) is a graph showing xenon adsorption isotherms at various temperatures with O₂ and N₂ isotherms at 25°C included for comparison.

15 Figure 3(b) is a graph showing isotheric heats of xenon adsorption at various loadings.

Figure 4 is a GC printout for xenon/air separation at 250°C on Ag-ETS-10.

Figure 5(a) shows a gas chromatographic profile obtained at 30°C with 30 ml/min helium carrier flow for Ar, O₂ and a 50%-50% mixture of Ar- O₂ on Ag-ETS-10.

20 Figure 5(b) shows a gas chromatographic profile obtained at 30°C with 30 ml/min helium carrier flow for Ar, O₂ and a 50%-50% mixture of Ar- O₂ on Ag-mordenite.

Figure 6(a) is a graph showing nitrogen, argon, and oxygen adsorption isotherms at 30°C on Ag-ETS-10 with an insert to expand the lower pressure regime.

5 Figure 6(b) is a graph showing nitrogen, argon, and oxygen adsorption isotherms at 30°C on Ag-mordenite with an insert to expand the lower pressure regime.

Detailed Description Of Preferred Embodiments

The present invention relates to metallic nanodots formed on ETS-10. When describing the present invention, all terms not defined herein have their common art-recognized
10 meanings. To the extent that the following description is of a specific embodiment or a particular use of the invention, it is intended to be illustrative only, and not limiting of the claimed invention. The following description is intended to cover all alternatives, modifications and equivalents that are included in the spirit and scope of the invention, as defined in the appended claims.

15 Although consistent terminology has yet to emerge, those skilled in the art generally consider "nanoclusters" to refer to smaller aggregations of less than about 20 atoms. "Nanodots" generally refer to aggregations having a size of about 100 nm or less. "Nanoparticles" are generally considered larger than nanodots, up to about 200 nm in size. In this specification, the term "nanodots" shall be used but is not intended to be a size-limiting
20 nomenclature, and thus may be inclusive of nanoclusters and nanoparticles.

The term "about" shall indicate a range of values 10% above and below the stated value, or preferably +/- 5%, or it may indicate the variances inherent in the methods or devices used to measure the value.

As used herein, "ETS zeolite" includes all forms of ETS zeolites including without
25 limitation, ETS-10. ETS zeolites, including ETS-10, are described fully in United States

5 Patent 5,011,591 *Large Pored Crystalline Titanium Molecular Sieve Zeolites*, the contents of which are incorporated in their entirety herein by reference. ETS zeolites are a family of stable crystalline titaniumsilicate molecular sieve zeolites which have a pore size of approximately 8 Angstrom units and a titania/silica mole ratio in the range from 2.5 to 25. They have a definite x-ray diffraction pattern and can be identified in terms of mole ratios of
10 oxides. ETS-10 is a molecular sieve zeolite having a crystal structure formed by orthogonal chains of corner sharing TiO_6 octahedra which are linked by corner sharing SiO_4 tetrahedra. This layout of structural units generates 12- and 7- membered ring channels which possess a free entrance of about 0.8×0.5 and 0.55×0.15 nm, respectively [22-24]. As used herein, "ETS-10" includes zeolitic materials that are isostructural with ETS-10.

15 In general terms, in one embodiment, metal nanodots may be formed on an ETS zeolite surface by ion-exchange of the metal cation into the ETS zeolite, followed by an activating step, resulting in the formation of metal nanodots. In one embodiment, the metal is one of silver, copper, nickel, gold or a member of the platinum group. As used herein, a "platinum group" metal is ruthenium, rhodium, palladium, osmium, iridium or platinum. Generally,
20 silver, gold and members of the platinum group are self-reducing. The use of salts of these metals will generally result in the formation of metal nanodots without the imposition of reducing conditions. However, the use of reducing conditions for such metals is preferable, if only to minimize oxidation of the metal. Generally, copper and nickel are reducible and their metal salts will generally result in the formation of metal nanodots upon activation in a
25 reducing atmosphere.

5 In a preferred embodiment, the metal comprises silver or nickel.

In one embodiment, silver ETS zeolites may be prepared by ion-exchange of ETS zeolites. For example, the ETS zeolites may be exposed to an excess of aqueous silver nitrate. In one embodiment, ion-exchange takes place at 80°C with stirring for 1 hour. The material may then be washed and dried. In one embodiment, the above steps are repeated one or more
10 times. The silver ions in the zeolite may then be converted to metallic silver nanodots, supported on the ETS zeolite, by an activation step. In one embodiment, the activation step may simply comprise the step of drying the material at room temperature. In a preferred embodiment, the activation step may comprise annealing the material at an elevated temperature, such as from 75°C to 500°C or higher, and preferably between about 75° to
15 about 400° C. The activation step may take from 1 to 4 hours, or longer. In one embodiment, the activating step is performed in a reducing environment.

In one embodiment, the nanodots have a size less than about 100 nm, for example less than about 50 nm, less than about 30 nm or less than about 20 nm. In one embodiment, a substantial majority of the metal nanodots formed have a particle size of less than about 15
20 nm and greater than about 5 nm, with a mean particle size about 10 nm.

In general, the size of the nanodots appears to be influenced by reducing or oxidizing conditions of the activating step. In one embodiment, the use of reducing conditions results in generally smaller nanodot sizes. Conversely, the use of mild oxidizing conditions, such as air, results in generally larger nanodot sizes.

5 Without being restricted to a theory, it is believed that the activating process causes the silver ions to migrate to the surface of the ETS zeolite, where they reside as nanodots rather than as large particles or sheets. The silver ions reduce to their metallic state, before or after nanodot formation. Although the exact mechanism of the nanodot formation is not known, and without restriction to a theory, the scale and uniform distribution are likely due to the
10 ability of ETS zeolite surface to attract non-polar species such as a pure metal. As a result, pure metals tend to stick to the surface of the ETS zeolite surface.

In a preferred embodiment, ETS-10 is the form of ETS zeolite used, and silver is the metal used to form the metallic nanodots in an Ag-ETS-10 complex.

Ag-ETS-10 zeolites may have many possible uses which exploit the macro and nano
15 properties of the metallic element. In one embodiment of a silver nanoparticulate material, it may be used as a novel anti-microbial agent. Ag-ETS-10 may be incorporated into bandages, wound dressings or the like, or incorporated into solutions, creams or ointments, or the like, to be used to prevent or treat microbial infections.

Further, while it is known that generally silver exchanged zeolites exhibit unusual
20 adsorption properties, especially toward the so called inert or rare gases, and Ar, Kr, Xe or Ra in particular, Ag-ETS-10 zeolites may provide more selective or stronger adsorption properties than prior art silver zeolites. Therefore, in one aspect, the invention may comprise the use of Ag-ETS zeolites to selectively adsorb a rare gas from a gaseous mixture or stream. The rare gas may be a member of group 18 of the periodic table, and may comprise Ar, Kr, Xe
25 or Rn.

5 Without restriction to a theory, the nature of rare gas adsorption in silver zeolites generally
may be related to the directional properties given by the d orbitals of silver ions [1]. Ag^+ ions
in silver zeolites react, upon heating, to generate clusters with a wide range of compositions
including metal nanoensembles and groupings which may be composed of a combination of
silver atom clusters and ions. The clusters can occupy different sites in the zeolitic structure
10 [25]. This variability in composition and location of the clusters results in materials which
can express many different colors (from white or light yellow to dark gray), dependent
upon the state of the silver and its thermal history [25-27].

Accordingly, in one embodiment of the invention, Ag-ETS zeolites have been
demonstrated to be selective for argon over oxygen under certain conditions. Therefore, in
15 one embodiment, Ag-ETS-10 zeolites may be used to generate substantially pure oxygen. In
another embodiment, Ag-ETS-10 zeolites have been demonstrated to interact strongly with
xenon, and have a high selectivity for xenon over nitrogen and oxygen.

Enhanced interaction between xenon and silver exchanged zeolites *X* and *Y* has been
reported, including xenon adsorption isotherms and xenon NMR [28-30]. The initial isosteric
20 heat of xenon adsorption for silver zeolites is uniformly higher than for their sodium analogs,
and a substantial displacement of the chemical shift has been observed in the ^{129}Xe NMR
spectrum with silver present. The adsorption capacity of xenon and krypton on silver
mordenite as well as 5A zeolite and activated carbon, especially at very low pressures [31].

Grosse et al. [32, 33] studied xenon adsorption and ^{129}Xe NMR in silver-exchanged X and
25 Y zeolites, reporting that xenon is adsorbed more strongly in the silver-exchanged zeolites

5 than in their sodium analogs. This stronger interaction was also seen in the displacement of
the chemical shifts of ^{129}Xe adsorbed on silver zeolites when compared to those of the sodium
starting materials. This was qualitatively explained by specific interactions of xenon with the
silver cations in the super-cages of the zeolites. It was also reported that the initial isosteric
heat of adsorption of xenon was 31 kJ/mol in silver-exchanged zeolite Y compared to 18.5
10 kJ/mol in the sodium form [34].

Xenon Adsorption

Xenon is present in ambient air at a concentration of 0.087 ppm. If it were economical to
use, xenon might find widespread application as an anesthetic, having been referred to as ideal
15 [35]. Recycling xenon gas could dramatically reduce its net cost in such applications. Xenon
is currently generally derived from air by distillation. Companies specializing in air
separation have developed techniques for xenon extraction from air [36-38]. Currently, most
of the xenon produced in the world is used in specialized lighting. Other applications include
nuclear medicine and laser applications. Characteristics of the xenon market and its
20 applications have been reviewed and summarized by Hammarland [39]. Most important,
xenon has high potential as an anesthetic gas [35] but its current high price prevents
widespread usage.

In current processes, a mixture of krypton and xenon is obtained from an oxygen stream in
air distillation. The krypton and xenon are then further separated by cryogenic methods. Due
25 to the high energy requirements of this cryogenic recovery, several alternative processes have
been proposed. Certain polymer membranes have shown promise for the separation of xenon

5 from air [40]. Efficient xenon selective adsorbents might allow not only more economical xenon capture from the atmosphere but could conceivably be employed to recapture and recycle xenon from an operating room environment, dramatically cutting its cost per use.

Argon Adsorption

10 Although the strength of the interaction between silver zeolites and noble gases decreases markedly in the order $Xe > Kr > Ar$, the sorption affinity for argon is still significant, and some silver zeolites possess the unique property of being measurably selective in adsorbing argon (vs. oxygen). The separation of argon and oxygen by adsorption-based methods is difficult due to the similar diameter and polarizability of the Ar atoms and O_2 molecules.

15 However, molecular sieves and microporous polymers with some degree of selectivity for oxygen are known and have been applied since the 1960s for the chromatographic resolution of Ar, O_2 , and N_2 and other analytical purposes [41-46]. Oxygen (over argon) kinetic selectivity in certain carbon adsorbents has been employed for the production of purified oxygen and argon by pressure swing adsorption (PSA) [47,48].

20 The preceding methods for the separation of oxygen and argon are based upon adsorbents that show selectivity for oxygen over argon. Silver mordenite has been reported to manifest at least some argon selectivity (vs. oxygen) [49]. Pressure swing adsorption simulations and experiments were successfully performed for the purification of oxygen from 95% O_2 to 5% Ar at 60-90 °C [49]. While silver mordenite appears to be the most widely reported zeolite-

25 based argon selective adsorbent, silver exchanged zeolite X [50], silver exchanged Li-Na-LSX

5 zeolite [51,52], silver exchanged zeolite A [53,54], Y, L, BEA, and ZSM-15 [28] have all been reported to show some degree of argon selectivity.

Nitrogen also interacts strongly with silver exchanged zeolites. The nitrogen adsorption capacity and isosteric heat of adsorption of fully exchanged zeolite Ag-X was found to be significantly higher than that of Na-X and Li-X [55]. This effect was explained by means of a
10 π -complexation mechanism, which would involve donation of the π -bond electrons of the N_2 molecule to the empty s orbital of Ag^+ , and back-donation of electrons from the d orbital of silver to the empty $7c$ -antibonding orbital of N_2 [55]. The basic concept for π -complexation was described first by Dewar [56]. The N_2/O_2 selectivity of Ag-X zeolite is also reported to be higher than for other cations. This effect has also been explained according to the π -
15 complexation theory. The π -antibonding electrons of the O_2 molecule do not allow the back-donation of electrons from the silver d orbitals. The bonding strength of N_2 is too strong for practical PSA separations. However, it has been reported that combining the potentials of lithium and silver in hybrid LiAg-X zeolite can be superior to Li-X for air separation under certain circumstances. It has also been reported that a small amount of substitution of Ag in
20 Li-X can improve N_2/O_2 separation properties [57]. Other silver exchanged zeolites, such as mordenite [58] and zeolite A [54], have been reported to have enhanced N_2 capacities and N_2/O_2 selectivities compared to materials without silver.

5 **Examples**

Example 1 – production of Ag-ETS-10

ETS-10 was synthesized under hydrothermal conditions as reported by Kuznicki in U.S. Patent 5,011,591, *Large Pored Crystalline Titanium Molecular Sieve Zeolites*, the entire contents of which are incorporated in their entirety herein by reference. The ETS-10 adsorbent was ion exchanged by adding 5 g of ETS-10 to 10 g of Silver Nitrate (Fisher, USP) in 50 g of deionized water. The mixture was heated to 80 °C for a period of 1 h. The silver treated material was filtered, washed with deionized water and the exchange procedure was repeated twice (for a total of three exchanges). The silver exchanged ETS-10 was dried at 80 °C. Elemental analysis indicated essentially quantitative silver exchanged with Ag constituting slightly more than 30% of the finished material.

Example 2 - Adsorption of Xenon – Experimental Parameters

Two adsorbents were examined, Na-ETS-10 and its silver exchanged counterpart Ag-ETS-10.

Inverse gas chromatography data were obtained on a Shimadzu GC 14-B apparatus. Adsorbents were packed into columns and pretreated under helium flow at 250 °C over night. Test gas samples were injected into the columns at pre-chosen temperature intervals. Corrected retention times for each gas at the test temperature are reported in Table 1 below.

TABLE 1: Chromatographic Data for Xenon and Air Traversing ETS-10 Based Adsorbent Columns at Various Temperatures and Projected Selectivities (α) of Xe/air (N₂) at 25 °C

sample	T [°C]	retention time [min]		α [mol/mol]	q_{st} [kJ/mol]		α (25 °C)
		air (N ₂)	Xe		air (N ₂)	Xe	
Ag-ETS-10	200	0.53	39.29	138	32.1	52.5	2903
	225	0.45	21.28	107			
	250	0.39	12.18	85			
Na-ETS-10	30	1.78	26.84	18	22.8	27.5	18.5
	50	1.20	14.70	16			
	70	0.88	9.40	16			
	100	0.62	4.45	13			

5

Mathematical analysis of GC data using the Clapeyron—Clausius equation [59] was performed, using Henry's law constants, to project xenon/ air (N₂) selectivities to room temperature. These projections were then compared to adsorption isotherms as described below.

10 Adsorption isotherms for Xe, N₂, and O₂ were obtained by gravimetric analysis using a Rubotherm magnetic suspension metal balance system (accuracy of ± 0.1 μ g) constructed to our specifications by VTI Corp. of Hialeah, Florida. Samples were activated at 150 °C under a vacuum of greater than 10^{-4} Torr for a period of 6 h.

Example 3 - Adsorption of Xenon – Results

15 Xenon adsorption isotherms were measured at various temperature increments (25, 60, 100, and 150 °C), and these isotherms were used to calculate isosteric heats of adsorption (q_{st}) as a function of adsorbate loading by plotting $\ln p$ vs $1/T$ [60].

On Na-ETS-10, xenon adsorption at 25 °C is nearly linear with pressure (see Figure 2).

However, silver exchange dramatically changes adsorption behavior, generating a steep isotherm

20 which reaches 6% weight loading by 0.5 Torr at 25 °C.

5 When low-pressure xenon isotherms are measured at temperatures between 25 and 150°C
(Figure 3a) adsorption is substantial, even at elevated temperatures. Comparative nitrogen and
oxygen isotherms (Figure 3a) infer substantial selectivity for the removal of xenon from air.
Using these isotherms, isosteric heats of adsorption for xenon at various adsorbate loadings
were calculated (Figure 3b). In the range of adsorbent loadings available, the values of q_{st}
10 varied with loading from 40 to greater than 90 kJ/mol adsorbed. Linear extrapolation to zero
loading gives a projected value of approximately 136 kJ/mol for the limiting isosteric heat of
adsorption. If correct, this is of the same magnitude as reported for Xe—F bond energies in
Xe—F₆ and Xe—F₄ [61].

 This interaction is much stronger than previously reported for Ag loaded classical zeolites
15 such as X and Y [33,34]. This strong interaction cannot be rationalized by classical zeolite
cation-adsorbate interactions or interactions with the zeolite framework. It is known that silver
cations in certain exchanged zeolites can be reduced to metal nanoparticles at temperatures as
low as 150 °C [62]. TEM images show the formation of what appears to be silver nanoparticles
on the ETS-10 surfaces (Figure 1). Nano-structured silver might be expected to maximize
20 silver's interaction energies with potential sorbates including xenon. The activated Ag-ETS-10
also lacks the yellow coloration generally associated with Ag⁺ ions in molecular sieves [63, 64,
65]. We presume the strong binding with xenon comes from its interaction with the silver
nanoparticles.

 The heat of adsorption calculated from isotherm modeling may appear to be unrealistically
25 high for a reversible physisorption process. However, both the shape of the isotherms and the
projected limiting heat of adsorption are strongly reminiscent of a polar molecule such as

5 water on a classical zeolite desiccant (such as zeolite X or zeolite A). Such isotherms and isosteric heat plots are usually associated with a finite population of very strong adsorption sites coupled with a large surface at lower binding energy. Zeolite desiccants form the basis of many regenerable (reversible) drying processes. Xenon adsorbed on Ag-ETS-10 can be completely removed by applying a vacuum at 150 °C.

10 Xenon interacts with Ag-ETS-10 so strongly that inverse gas chromatography experiments required elevated temperatures for practical run times. Figure 4 depicts the GC printout of a 50—50 mixture of xenon and air injected in a 10" x 1/4" column of Ag-ETS-10 at 250 °C under 30 cm³/min flow of helium. Air traverses the column quickly, essentially in the time of an inert gas, whereas xenon shows substantial retention, even at 250 °C. Both xenon and air
15 rapidly traverse an Na-ETS-10 column under these conditions. Table 1 lists chromatographic data for Ag-ETS-10 in the temperature regime of 200—250 °C and Na-ETS-10 from 30 to 100 °C. Projections of these data to room temperature (25 °C) indicate a xenon/air (N₂) selectivity of approximately 18 for Na-ETS-10 which rises to nearly 3000 in the silver form. Such extremely selective xenon adsorbents might be employed to effectively scrub an
20 operating room's air to recover (and recycle) valuable xenon anesthetics.

The indicated heat of adsorption for xenon from the inverse gas chromatography experiments (at 52.5 kJ/mol) is substantially less than the projected 130+ kJ/mol from adsorption isotherms. We do not know whether this is due to our adsorption modeling being incorrect for this new system or if GC data are not representative of the Henry's law regime
25 for such a strong adsorbent. Both the relative symmetry of the xenon peaks and their small variations in retention with injection size support the GC binding energies while adsorption

5 isotherms qualitatively and quantitatively support the higher value. Irrespective, both techniques indicate unprecedented selectivity for the adsorption of xenon from air (N₂). It must be noted that a full cc injection of xenon takes over 12 min to pass through a column containing only about 3 g of adsorbent at 250 °C and 30 cm³/min carrier flow. Projected Henry's law constants from the chromatographic data indicate that this passage time would
10 approach 1 month at room temperature.

From both isothermal and chromatographic data, it is clear that silver ETS-10 is an excellent adsorbent for xenon. Therefore, this may have utility in xenon recovery and purification.

Example 4 – Argon Adsorption – Experimental Parameters

15 A comparative study was done between Ag-mordenite and Ag-ETS-10. In order to obtain Ag-mordenite, hydrogen mordenite (from Zeolyst Corp.) was silver exchanged in a manner similar to that described for ETS-10. With its inherently lower exchange capacity, the silver loading on the mordenite was found to be approximately 8% by elemental analysis.

Inverse gas chromatography experiments were performed using a Varian CP 3800 gas
20 chromatograph (GC). Test adsorbents were packed into 10" long, 1/4" OD copper columns. Typical columns contained approximately 3 g of test adsorbent. The columns were installed in the Varian CP 3800 GC and were treated at 350 °C for 16 h under 30 ml/min helium carrier flow. The test gas samples constituted 1 cc injection of Ar, O₂, and 50-50% mixtures of O₂-Ar and were performed at 30 °C with 30 ml/min helium carrier flow.

5 Low pressure (up to 120 kPa) nitrogen, oxygen, and argon adsorption isotherms were measured at 30 °C in a Micromeritics (ASAP 2010) volumetric adsorption system. Test samples were dried (150 °C for Ag-ETS-10 and 350 °C for Ag-mordenite) for 6 h under a vacuum of greater than 10^{-4} Torr. Adsorption isotherms were fitted to the classical Langmuir equation:

$$10 \quad n = \frac{n_m \cdot K_L \cdot p}{1 + K_L \cdot p},$$

Where n is the amount adsorbed (mmol g^{-1}) at the pressure p (kPa), and n_m and K_L are the fitting parameters. According to the Langmuir model, n_m is interpreted as the mono-layer coverage (mmol/g), and the product $n_m \cdot K_L$ ($\text{mmol g}^{-1} \text{ kPa}^{-1}$) equals the Henry's law constant at low loading, when $p \rightarrow 0$. The selectivity (α) was calculated from the pure gas Langmuir isotherms as:

$$\alpha(A/B) = \frac{K_A}{K_B},$$

Where α (A/B) is the selectivity of gas A over gas B expected at low loadings and expressed as the ratio of their respective Henry's law constants K_A and K_B ($K = n_m \cdot K_L$).

20 **Example 5 – Argon Adsorption - Results**

Color changes were noted for both Ag-ETS-10 and Ag-mordenite during activation. Ag-ETS-10 is initially light brown and becomes dark gray after heating to 150 °C in vacuum. Ag-mordenite changes from a light greenish yellow to a light gray with activation at 350 °C. The

5 color changes infer a change in the state of silver during activation, presumed to be partial or total reduction to metal. Mordenite required the higher temperature for complete activation.

Figures 5a and 5b show gas chromatographic profiles for Ag-ETS-10 and Ag-mordenite with injections of both a 50-50% mixture of O₂-Ar and injections of the pure gases. The retention times for pure argon are larger than for pure oxygen in both Ag-ETS-10 and Ag-
 10 mordenite, indicating an affinity for argon over oxygen, although chromatographic splitting is much more obvious for Ag-ETS-10 when the mixed gases are injected.

Figures 6a and 6b show nitrogen, argon, and oxygen adsorption isotherms for Ag-ETS-10 and Ag-mordenite together with their Langmuir fitting curves up to a pressure of 120 kPa. A blow-up of isotherm data at lower pressures (up to 8 kPa) is included as an insert. Up to 120
 15 kPa, all experimental isotherms fit the Langmuir model well. The parameters of these Langmuir isotherms are listed in Table 2, together with their standard deviations (σ):

$$\sigma = \frac{\sum(n_{\text{exp}} - n_{\text{calc}})}{N - m},$$

Where n_{exp} is the experimentally measured adsorption (mmol g⁻¹) at pressure p (kPa) and n_{calc} is the adsorption calculated from the Langmuir equation at the same pressure. N is the
 20 number of experimental points taken and m is the number of fitting parameters (2 for the Langmuir equation).

Langmuir parameters for the adsorption data in the range of 0–120 kPa

Langmuir (0–120 kPa)		Ag-ETS-10	Ag-mordenite
Nitrogen	n_m (mmol g ⁻¹)	0.53865	0.62092
	$K_L \cdot n_m$ (mmol kPa ⁻¹ g ⁻¹)	0.02546	0.01171
	$\sigma \cdot 10^3$	0.108	0.148
Argon	n_m (mmol g ⁻¹)	0.73262	0.84651
	$K_L \cdot n_m$ (mmol kPa ⁻¹ g ⁻¹)	0.00302	0.00272
	$\sigma \cdot 10^3$	0.002	0.005
Oxygen	n_m (mmol g ⁻¹)	0.98753	0.93305
	$K_L \cdot n_m$ (mmol kPa ⁻¹ g ⁻¹)	0.00202	0.00218
	$\sigma \cdot 10^3$	0.004	0.001
	α (N ₂ /Ar)	8.44	4.30
	α (N ₂ /O ₂)	12.58	5.36
	α (Ar/O ₂)	1.49	1.25

5

The calculated Langmuir adsorption isotherms were used to predict the selectivity of Ag-ETS-10 and Ag-mordenite for nitrogen, argon, and oxygen. The resulting selectivities for the Henry's law limiting region are included in Table 2. Both Ag-ETS-10 and Ag-mordenite demonstrate some selectivity for argon over oxygen at atmospheric pressure, and this is magnified at low pressure, especially in the case of Ag-ETS-10, which reaches a selectivity of 1.49 at its limit. Both materials show strong selectivity for nitrogen over oxygen and argon at low pressures, especially Ag-ETS-10 where the limiting N₂/O₂ selectivity exceeds 10. Considering that Ag-ETS-10 is approximately twice as dense as Ag-mordenite, differences in actual bed selectivities would probably be greater than indicated by the isotherms.

15

From chromatographic, volumetric and gravimetric isotherm measurements, both Ag-ETS-10 and Ag-mordenite demonstrate adsorptive selectivity for argon over oxygen at 30 °C over a wide range of pressures. Both adsorbents demonstrate somewhat higher capacity for oxygen than for argon at atmospheric pressure (1.2–1.3 times). This increases with decreasing pressure, especially in the case of Ag-ETS-10, where it reaches 1.49 at the Henry's law limit.

20

Ag-mordenite has been proposed as useful adsorbent for the production of high purity oxygen (>99%) from a previously enriched oxygen stream (from PSA air separation) containing

5 approximately 95% O₂ and 5% Ar. With its substantially higher Ar/O₂ selectivity at low argon partial pressures, Ag-ETS-10 is a suitable material to improve O₂ generation under these conditions.

REFERENCES

10 The following references are referred to in square brackets above, and the entire contents of these references are incorporated herein as if reproduced in their entirety.

[1] R. Jin, Y. Cao, E. Hao, G.C. Metraux, G.C. Schatz, C.A. Mirkin, *Nature* 425 (2003) 287.

[2] R. Jin, Y. Cao, C.A. Mirkin, K.L. Kelly, G.C. Schatz, J.G. Zheng, *Science* 294 (2001) 1901.

15 [3] A. Callegari, D. Tonti, M. Chergui, *Nano Lett.* 3 (2003) 1565.

[4] Y. Sun, B. Mayers, Y. Xia, *Nano Lett.* 3 (2003) 675.

[5] Y. Sun, Y. Xia, *Adv. Mater.* 15 (2003) 695.

[6] S. Chen, D.L. Carroll, *Nano Lett.* 2 (2002) 1003.

[7] Y. Zhou, C.Y. Wang, Y.R. Zhu, Z.Y. Chen, *Chem. Mater.* 11 (1999) 2310.

20 [8] M.J. Edmondson, W. Zhuo, S.A. Sieber, I.P. Jones, I. Gameson, P.A. Anderson, P.P. Edwards, *Adv. Mater.* 13 (2001) 1608.

[9] C.R. Li, X.N. Zhang, Z. Zhang, *Mater. Lett.* 58 (2004) 27.

[10] L.M. Worboys, P.A. Anderson, in: E. van Steen, L.H. Callanan, M. Claeys (Eds.), *Recent Advances in the Science and Technology of Zeolites and Related Materials, Parts A, B,C,*

25 *Studies in Surface Science and Catalysis*, vol. 154, 2004, p. 931.

[11] M. Tsapatsis, *AIChE J.* 48 (2002) 654.

[12] R. Strohal, M. Schelling, M. Takacs, W. Jurecka, U. Gruber, F. Offner, *J. Hospital Infect.* 60 (2005) 226.

[13] R.E. Burrell, L.R. Morris, P.S. Apte, S.B. Sant, K.S. Gill, US Patent 5,837,275 (1998).

30 [14] G.S. Metraux, C.A. Mirkin, *Adv. Mater.* 17 (2005) 412.

[15] L.R. Gellens, W.J. Mortier, J.B. Uytterhoeven, *Zeolites* 1 (1981) 85.

- 5 [16] V.S. Gurin, V.P. Petranovskii, N.E. Bogdanchikova, *Mater. Sci. Eng. C* 19 (2002) 327.
 [17] V.S. Gurin, V.P. Petranovskii, N.E. Bogdanchikova, *Mater. Sci. Eng. C* 23 (2003) 81.
 [18] V.S. Gurin, V.P. Petranovskii, M.-A. Hernandez, N.E. Bogdanchikova, A.A. Alexeenko, *Mater. Sci. Eng. A* 391 (2005) 71.
 [19] G. Bagnasco, P. Ciambelli, E. Czarán, J. Rapp, G. Russo, in: P.A. Jacobs, D.
- 10 Forschungsgemeinschaft (Eds.), *Metal Microstructures in Zeolites*, Elsevier, Amsterdam, 1982.
 [20] S.J. Cho, J.E. Yie, R. Ryoo, *Catal. Lett.* 71 (2001) 163.
 [21] V. Alt, T. Bechert, P. Steinrücke, M. Wagener, P. Seidel, E. Dingeldein, E. Domann, R. Schnettler, *Biomaterials* 25 (2004) 4383.
- 15 [22] M.W. Anderson, O. Terasaki, T. Oshuna, A. Philippou, S.P. Mackay, A. Ferreira. J. Rocha and S. Lidin, *Nature (London)* 1994, 367, 347.
 [23] M.W. Anderson, O. Terasaki, T. Oshuna, P.J.O. Malley, A. Philippou, S.P. Mackay, A. Ferreira. J. Rocha and S. Lidin *Philos. Mag. B.*, 1995, 71, 813.
 [24] J.M. Thomas, M.W. Anderson, P.A. Wright and J. Rocha *J. Phys. Chem.*, 1996, 100, 449.
- 20 [25] T. Sun, K. Seff, *Chem. Rev.* 94 (1994) 857.
 [26] N.D. Hutson, B.A. Reisner, R.T. Yang, B.H. Toby, *Chem. Mater.* 12 (2000) 3020.
 [27] J. Sebastian, R.V. Jasra, *Ind. Eng. Chem. Res.* 44 (2005) 8014.
 [28] R. Grosse, R. Burmeister, B. Boddenberg, A. Gedeon, J. Fraissard, *J. Phys. Chem.* 95 (1991) 2443
- 25 [29] R. Grosse, A. Gedeon, J. Watermann, J. Fraissard, B. Boddenberg, *Zeolites* 12 (1992) 909.
 [30] J. Watermann, B. Boddenberg, *Zeolites* 13 (1993) 427.
 [31] K. Munakata, S. Kanjo, S. Yamatsuki, A. Koga, D. Ianovski, *J. Nucl. Sci. Technol.* 40 (2003) 695.
- 30 [32] Grosse, R.; Burmeister, R.; Boddenberg, B.; Gedeon, A.; Fraissard, *J. J. Phys. Chem.* 1991, 95, 2443.
 [33] Grosse, R.; Gedeon, A.; Watermann, J.; Fraissard, J.; Boddenberg, B. *Zeolites* 1992, 12, 909.
 [34] Watermann, J.; Boddenberg, B. *Zeolites* 1993, 13, 427.

- 5 [35] Lynch, C.; Baum, J.; Tenbrinck, R. *Anesthesiology* 2000, 92, 865.
- [36] Shino, M.; Takano, H.; Nakata J.; Noro, K. Production process of xenon. U.S. Patent 4,874,592, 1989.
- [37] Cheung, H.; Couche, M. R.; Dray, J. R. Xenon production system. U.S. Patent 5,069,698, 1991.
- 10 [38] Agrawal, R.; Farrell, B. E. Cryogenic production of krypton and xenon from air. U.S. Patent 5,122,173, 1992.
- [39] Hammarland, N. *Nucl. Instrum. Methods Phys. Res., Sect. A* 1992, 316, 83.
- [40] Jensvold, J. A.; Jeanes, T. O. Membrane for separation of xenon from oxygen and nitrogen and method for using same. U.S. Patent 6,168,649, 2001.
- 15 [41] E.W. Lard, R.C. Horn, *Anal. Chem.* 32 (1960) 878.
- [42] K. Jones, P. Halford, *Nature* 202 (4936) (1964) 1003.
- [43] J.A.J. Walker, *Nature* 209 (5019) (1966) 197.
- [44] G.E. Pollock, D. O'Hara, *J. Chromatogr. Sci.* 22 (1984) 343.
- [45] G.E. Pollock, *J. Chromatogr. Sci.* 24 (1986) 173.
- 20 [46] P.J. Maroulis, C.G. Coe, *Anal. Chem.* 61 (1989) 1112.
- [47] S.U. Rege, R.T. Yang, *Adsorption* 6 (2000) 15.
- [48] X. Jin, A. Malek, S. Farooq, *Ind. Eng. Chem. Res.* 45 (2006) 5775.
- [49] K.S. Knaebel, A. Kandybin, US Patent 5,226,933, 1993.
- [50] A.I. Kandybin, R.A. Anderson, D.L. Reichley, US Patent 5,470,378,
- 25 1995.
- [51] R.L. Chiang, R.D. Whitley, J.E. Ostroski, D.P. Dee, US Patent 6,432,170 B1, 2002.
- [52] D.P. Dee, R.L. Chiang, E.J. Miller, R.D. Whitley, US Patent 6,544,318 B2, 2003.
- [53] J. Sebastian, R.V. Jasra, US Patent 6,572,838 B1, 2003.
- [54] J. Sebastian, R.V. Jasra, *Chem. Commun.* (2003) 268.
- 30 [55] R.T. Yang, Y.D. Chen, J.D. Peck, N. Chen, *Ind. Eng. Chem. Res.* 35 (1996) 3093.
- [56] M.J.S. Dewar, *Bull. Soc. Chim. Fr.* (1951) C71.
- [57] N.D. Hutson, S.U. Rege, R.T. Yang, *AIChE J.* 45 (1999) 714.
- [58] I. Salla, P. Salagre, Y. Cesteros, F. Medina, J.E. Sueiras, *J. Phys. Chem. B* 108 (2004)

5 5359.

[59] Diaz, E.; Ordfez, S.; Vega, A.; Coca, J. *Thermochim. Acta* 2005, 434, 9.

[60] Zangwill, A. *Physics at Surfaces*; Cambridge University Press: Cambridge, 1988; pp 192--194.

[61] Huheey, J. E. *Inorganic chemistry*, 3rd ed.; Harper & Row: New York, 1983; Appendix
10 E.

[62] Kuznicki, S. M.; Kelly, D. J. A.; Bian, J.; Lin, C. C. H.; Liu, Y.; Chen, J.; Mitlin, D.; Xu,
Z. Micropor. Mesopor. Mater. in press.

[63] Sun, T.; Seff, K. *Chem. Rev.* 1994, 94, 857.

[64] Hutson, N. D.; Reisner, B. A.; Yang, R. T.; Toby, B. H. *Chem. Mater.* 2000, 12, 3020.

15 [65] Sebastian, J.; Jasra, R. V. *Ind. Eng. Chem. Res.* 2005, 44, 8014.

20

25

5 WHAT IS CLAIMED:

1. A method of forming surface accessible metal nanodots having a size less than about 100 nm, comprising the steps of:
 - (a) performing ion-exchange with a solution of the metal ions and an ETS zeolite;
and
 - 10 (b) activating the ion-exchanged ETS zeolite.
2. The method of claim 1 wherein the ETS zeolite is ETS-10.
3. The method of claim 1 wherein the metal comprises silver, copper, nickel, gold or a member of the platinum group.
4. The method of claim 3 wherein the metal comprises silver.
- 15 5. The method of claim 1 wherein the activation step is performed under reducing conditions.
6. The method of claim 1 wherein the activating step is performed under oxidizing conditions.
7. The method of claim 1 wherein the activating step is performed at a temperature
20 greater than about 75 °C and less than about 500 °C.
8. The method of claim 7 wherein the activating step is performed at a temperature between about 75° and 400° C.
9. The method of claim 1 wherein the ion-exchange occurs with an excess of metallic ions.
- 25 10. An ETS-10 supported metal nanoparticulate material, comprising surface-accessible metal nanodots, having a particle size less than about 100 nm.

- 5 11. The material of claim 9 wherein the nanodots have a particle size less than about 50 nm.
12. The material of claim 10 wherein the nanodots have a particle size less than about 30 nm.
- 10 13. The material of claim 11 wherein the nanodots have a particle size less than about 20 nm.
14. The material of claim 12 wherein the nanodots have a particle size less than about 15 nm and greater than about 5 nm.
15. The material of claim 9 wherein the metal comprises silver, copper, nickel, gold or a member of the platinum group, or or mixtures thereof
- 15 16. The material of claim 14 wherein the metal comprises silver or nickel.
17. The material of claim 15 wherein the metal comprises silver.
18. A method of extracting xenon from a gas stream containing xenon using metal nanodots formed from a process as claimed in claim 1, or a material comprising metal nanodots claimed in claim 9, comprising the step of exposing the nanodots to air
20 containing xenon.
19. A method of extracting argon from a gas stream containing argon using metal nanodots formed from a process as claimed in claim 1, or a material comprising metal nanodots claimed in claim 9, comprising the step of exposing the nanodots to the oxygen stream containing argon.
- 25 20. The method of claim 18 wherein the oxygen stream comprises a previously enriched oxygen stream.
21. The method of claim 19 wherein the ratio of oxygen to argon in the oxygen stream is about 95% to 5%.

- 5 22. A method of extracting radon from a gas stream containing radon using metal nanodots formed from a process as claimed in claim 1, or a material comprising metal nanodots claimed in claim 9, comprising the step of exposing the nanodots to the oxygen stream containing radon.
- 10 23. A method of preventing or treating an infection in a body part by contacting the body part with metal nanodots formed from a process as claimed in claim 1, or a material comprising metal nanodots claimed in claim 9.

Figure 1

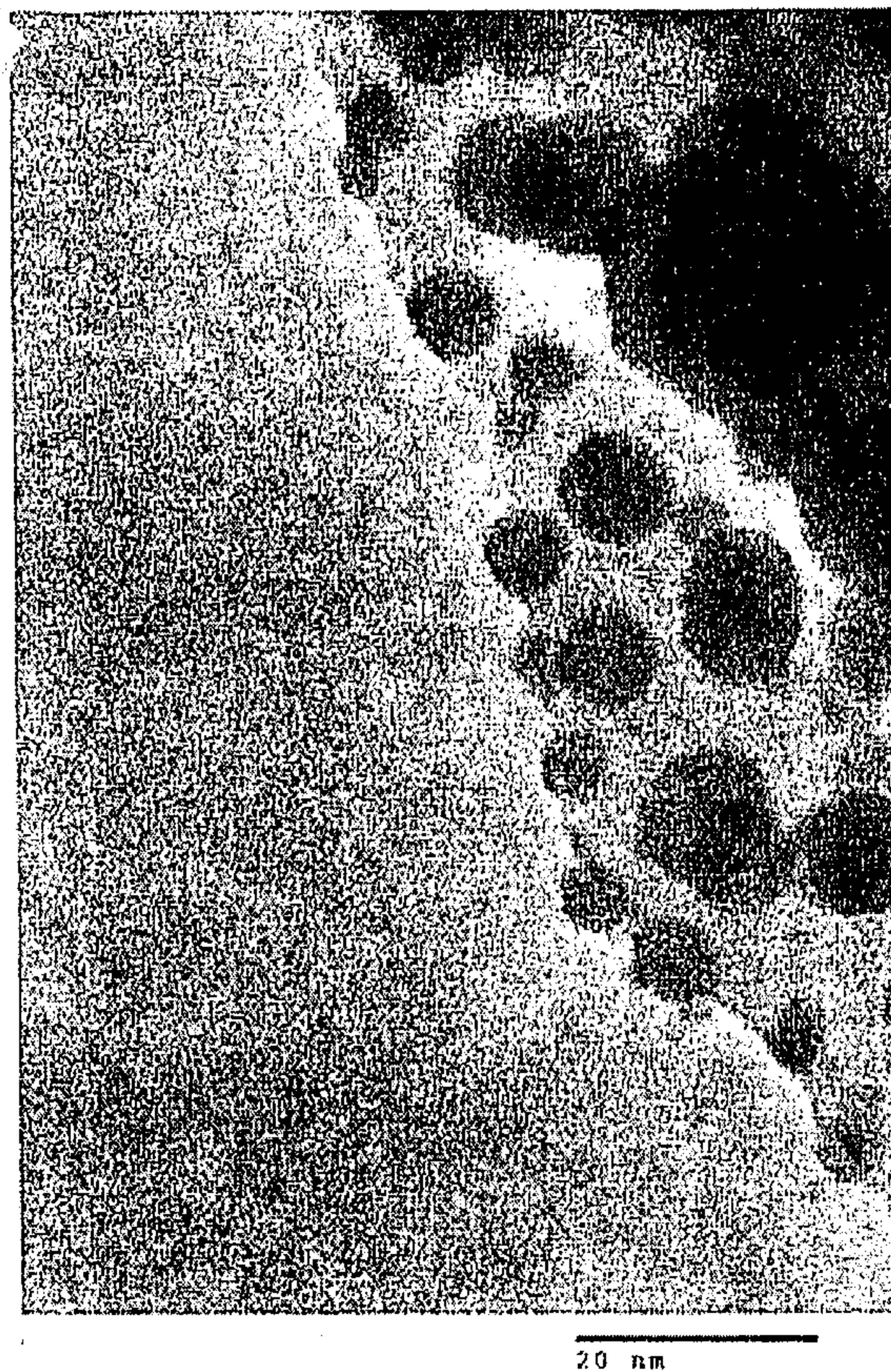


Figure 2

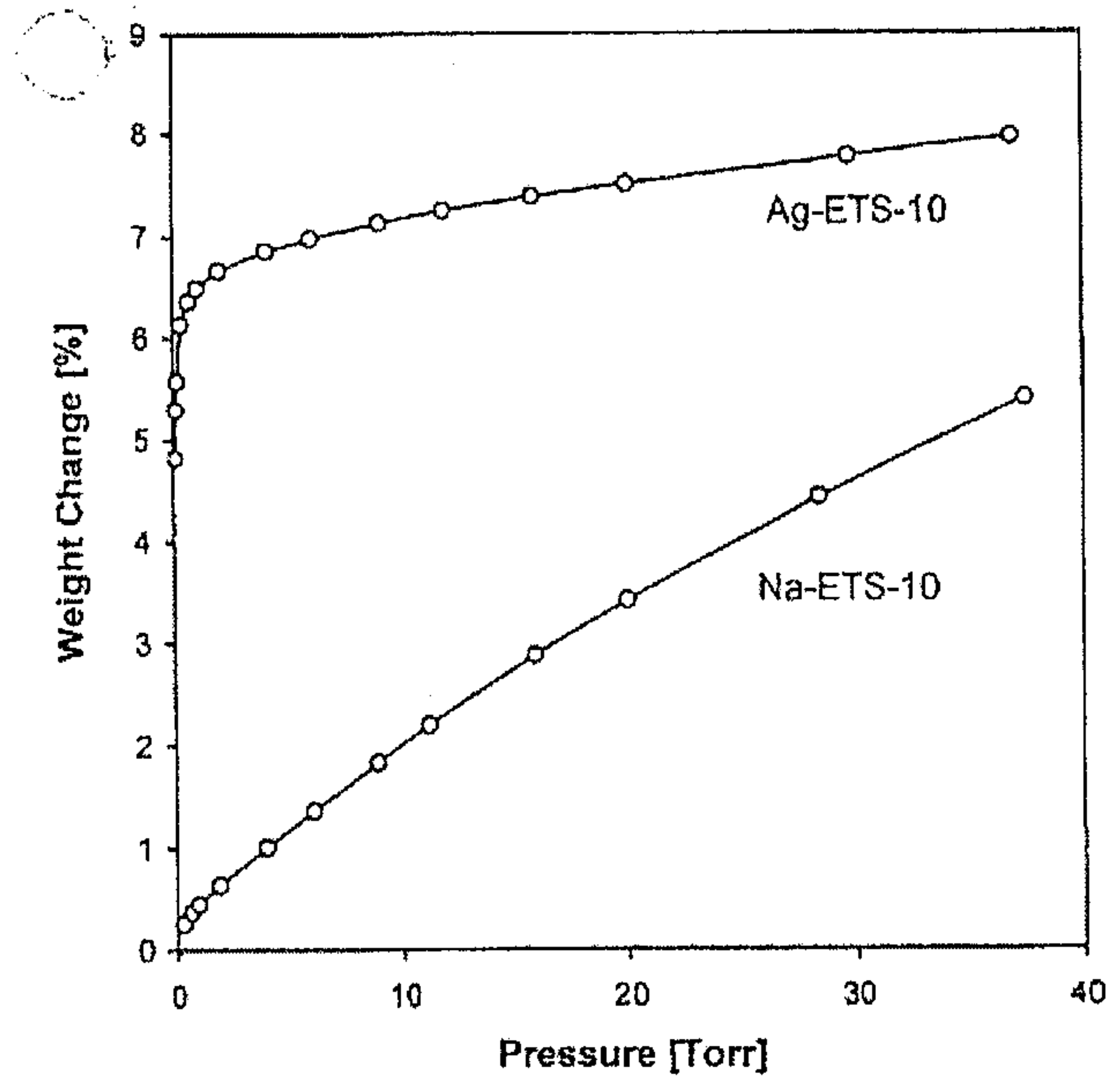


Figure 3a

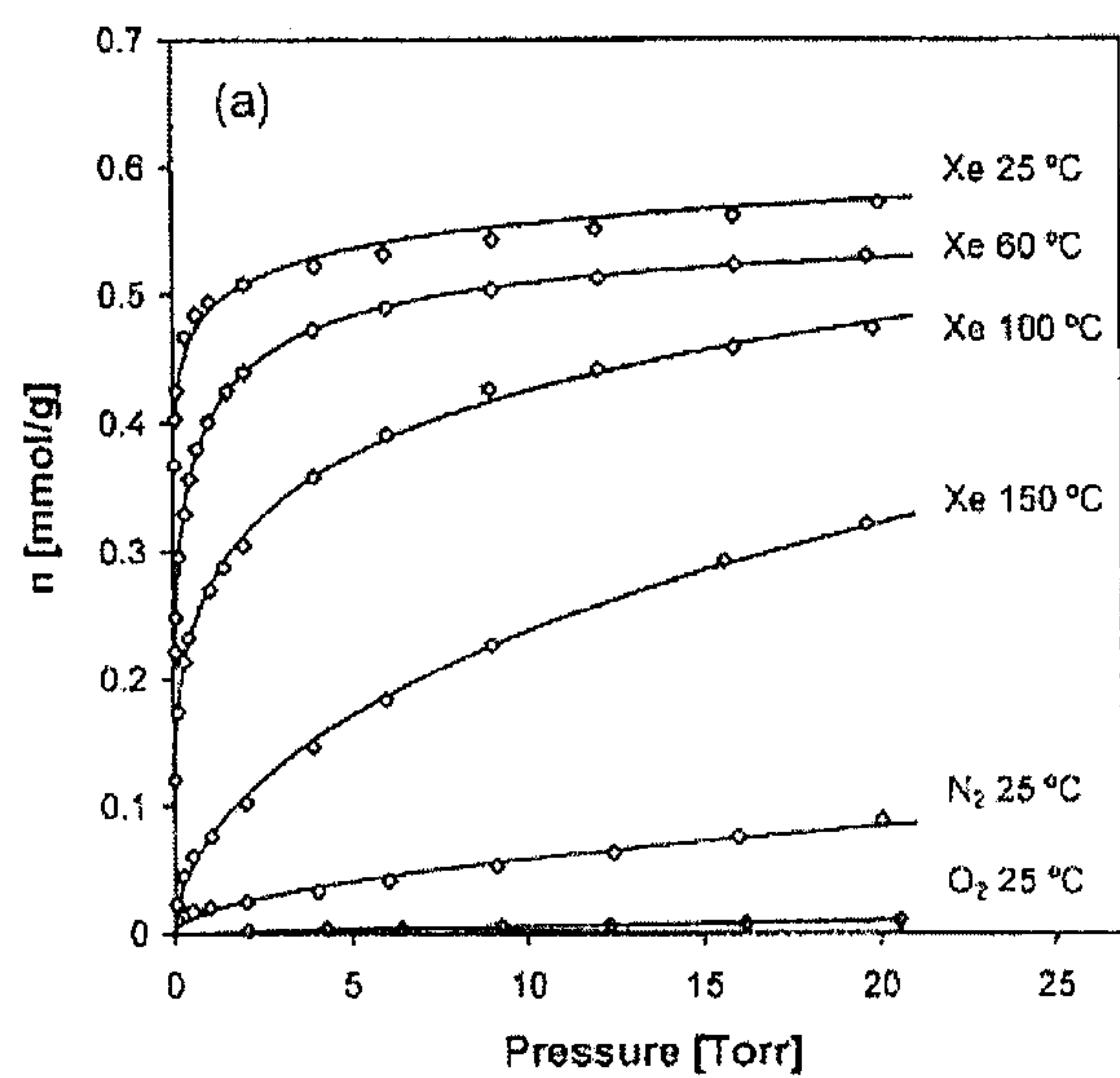


Figure 3b

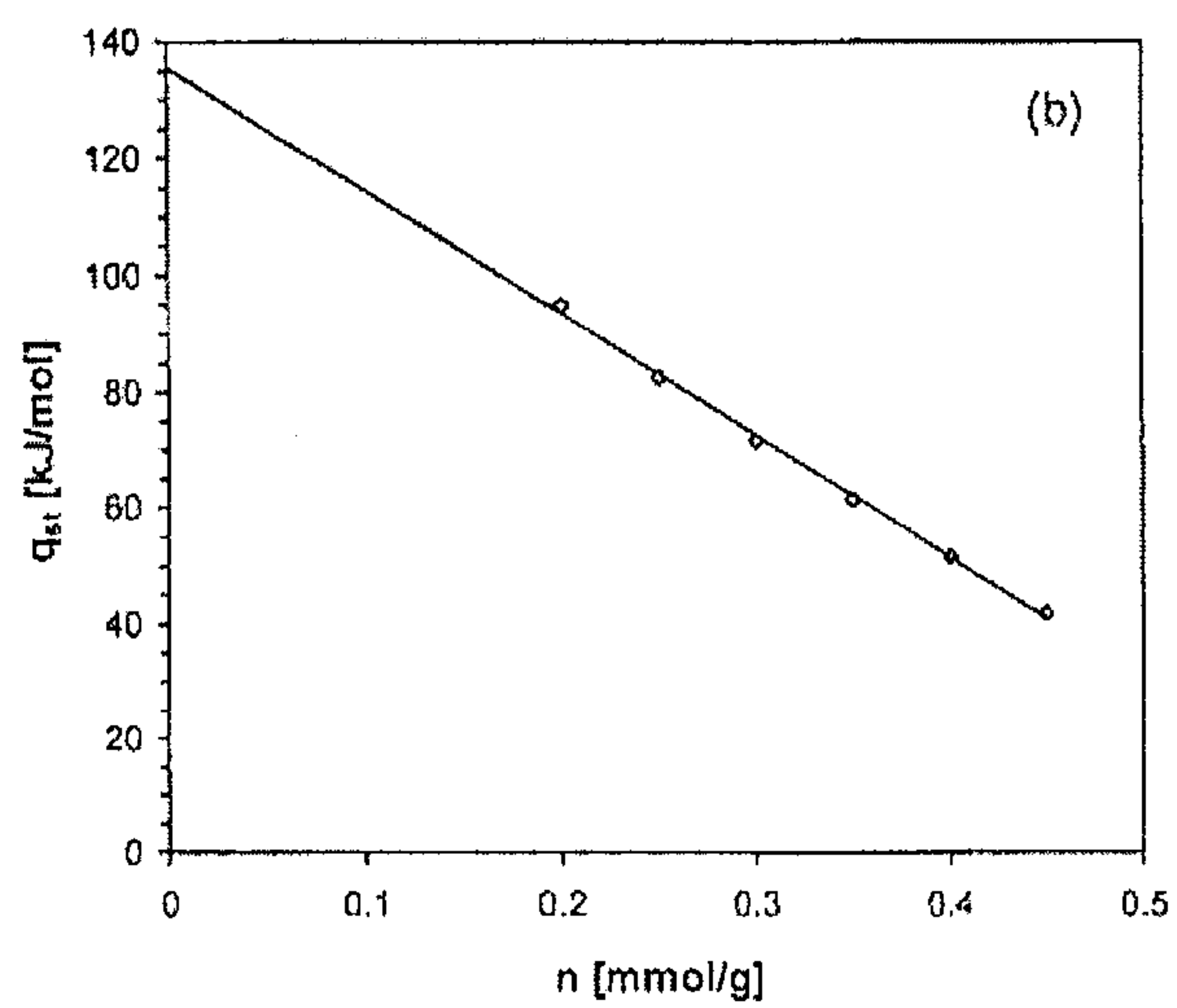


Figure 4

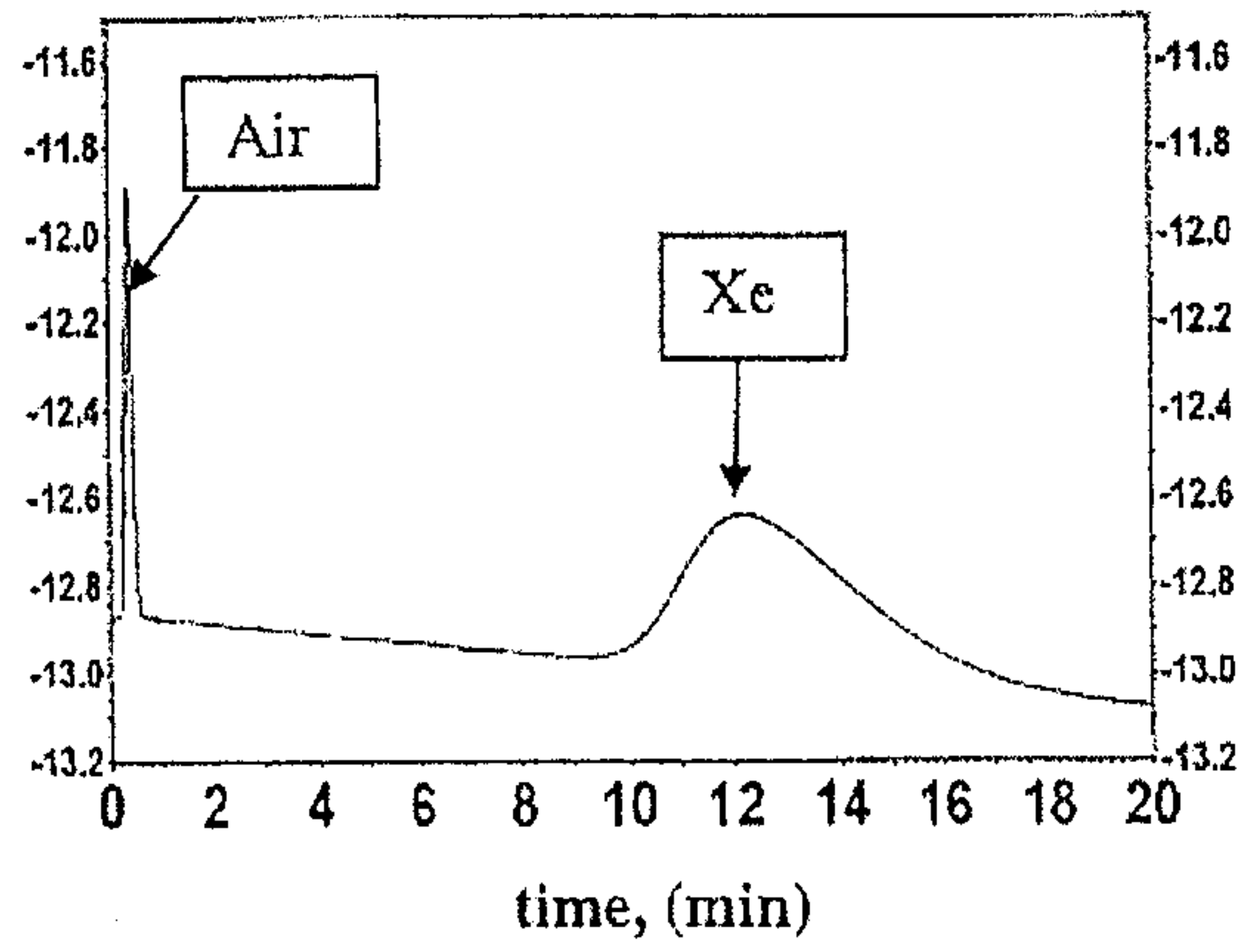


Figure 5a

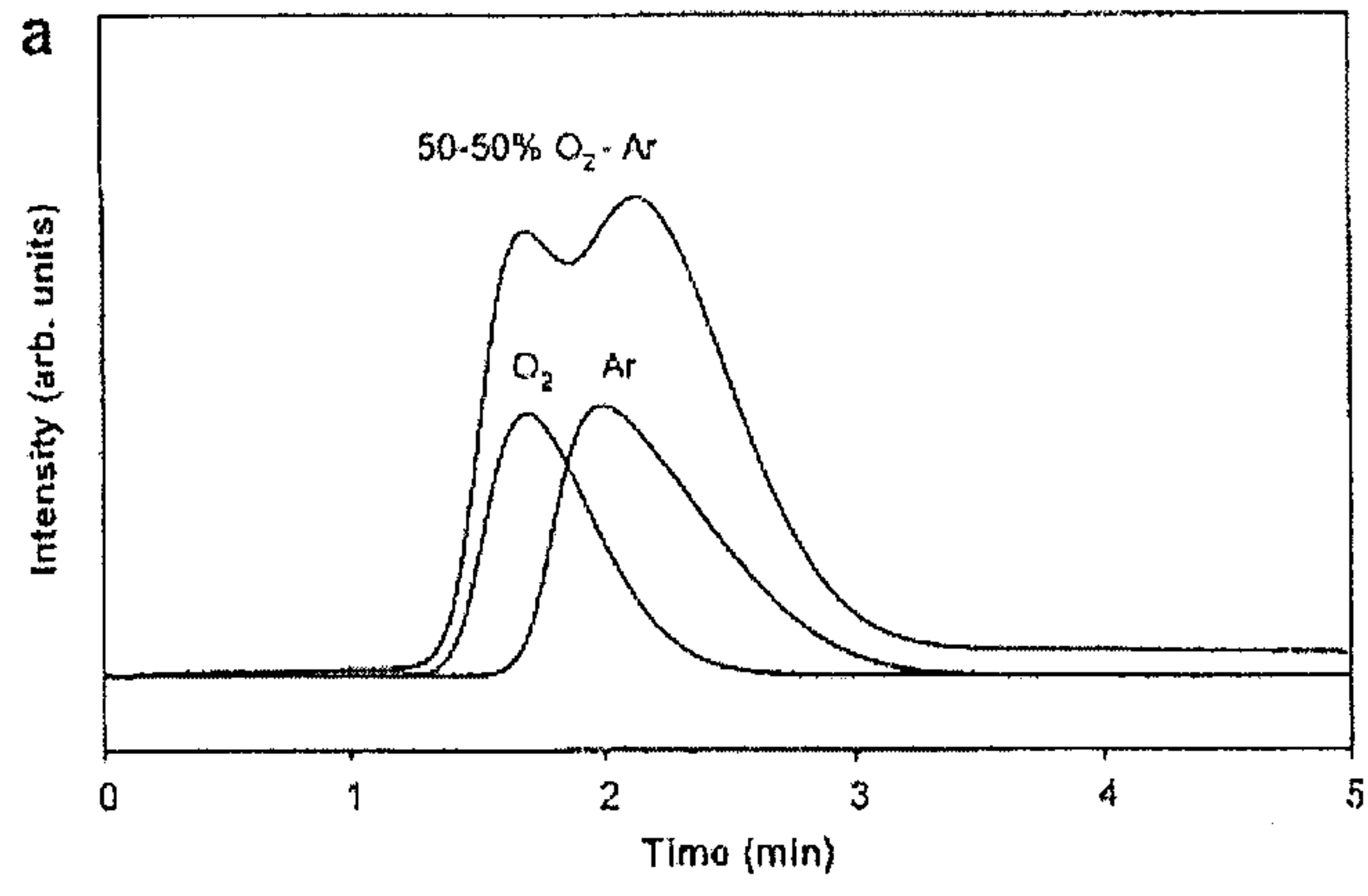


Figure 5b

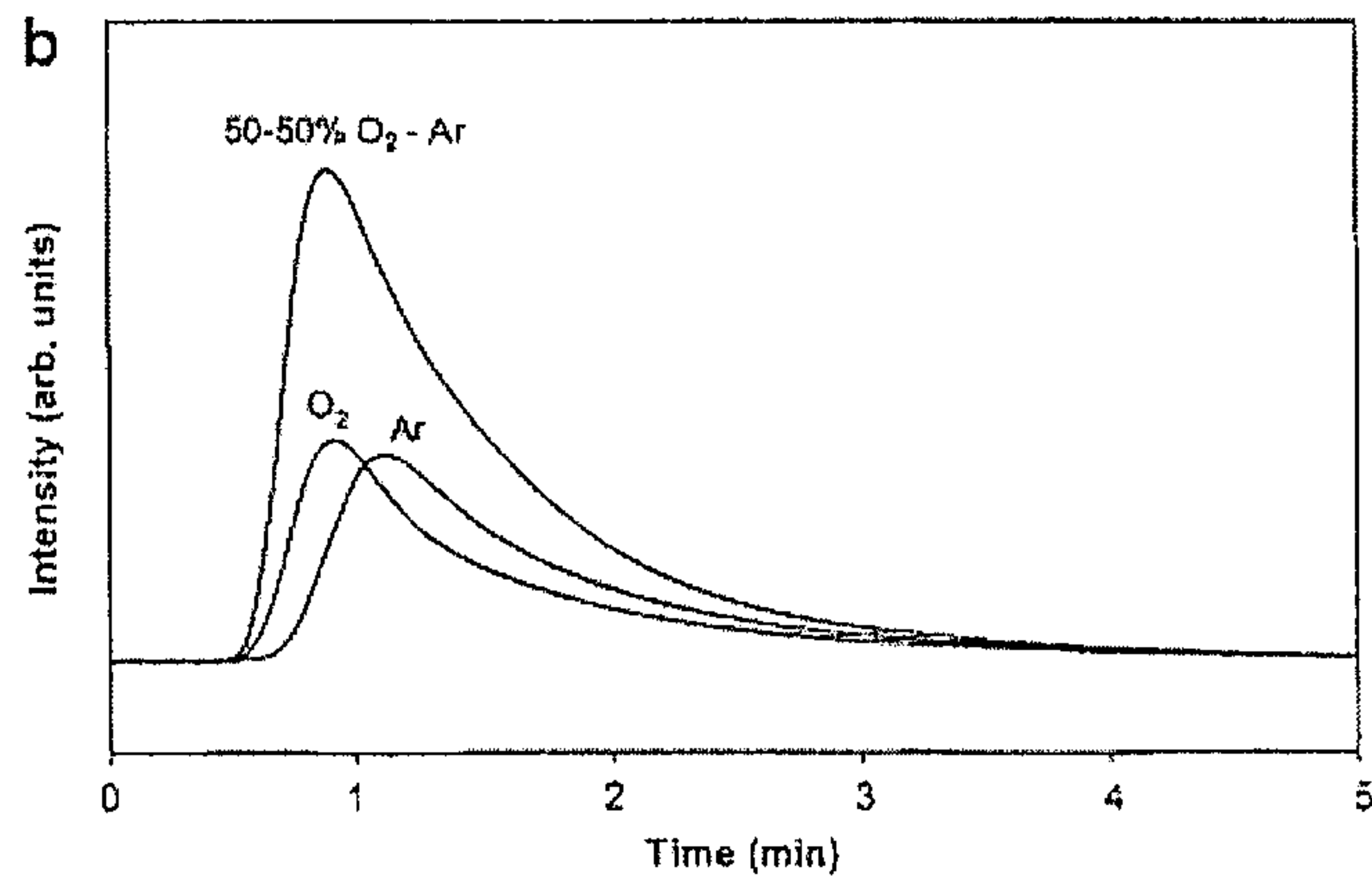


Figure 6a

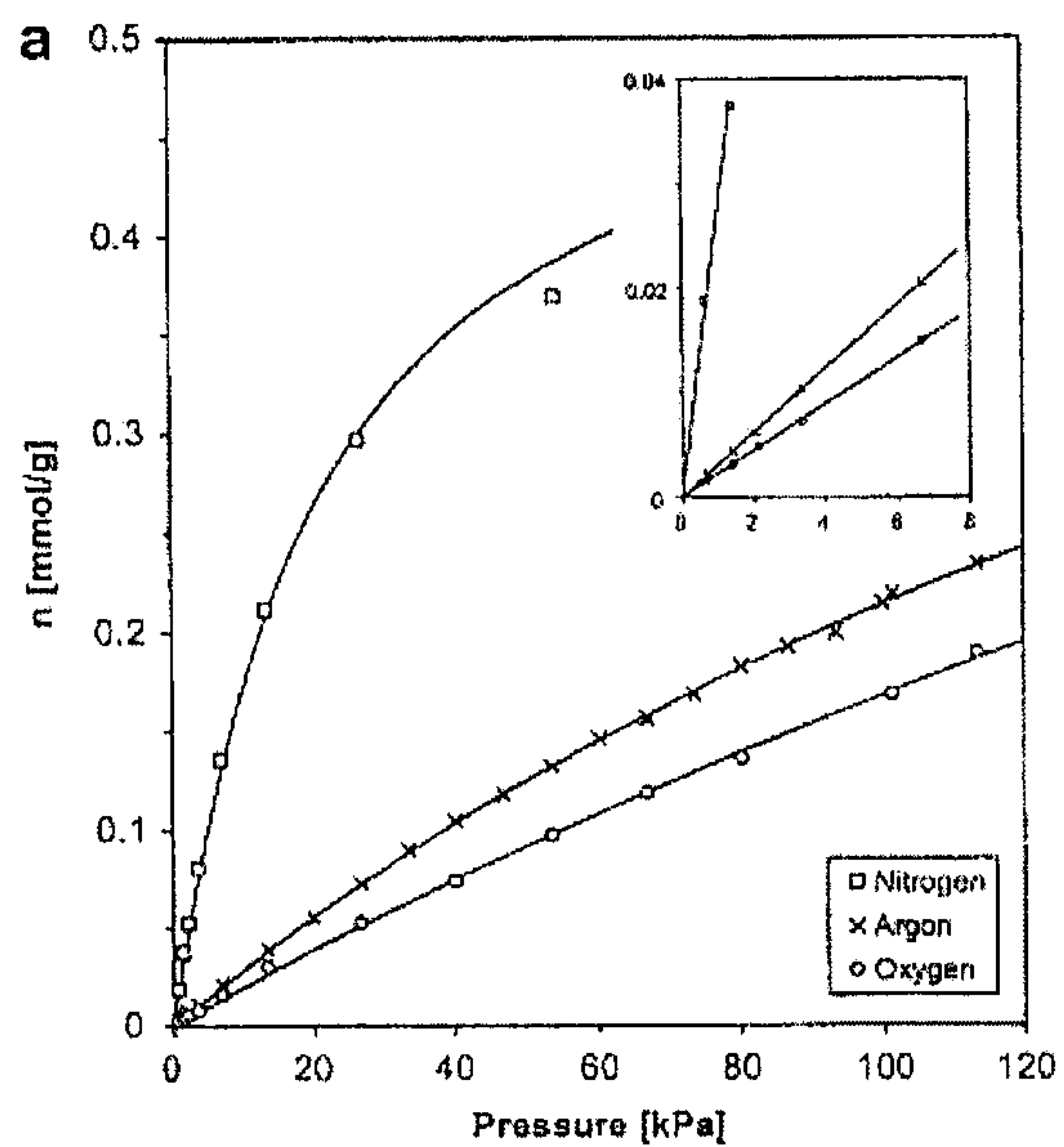
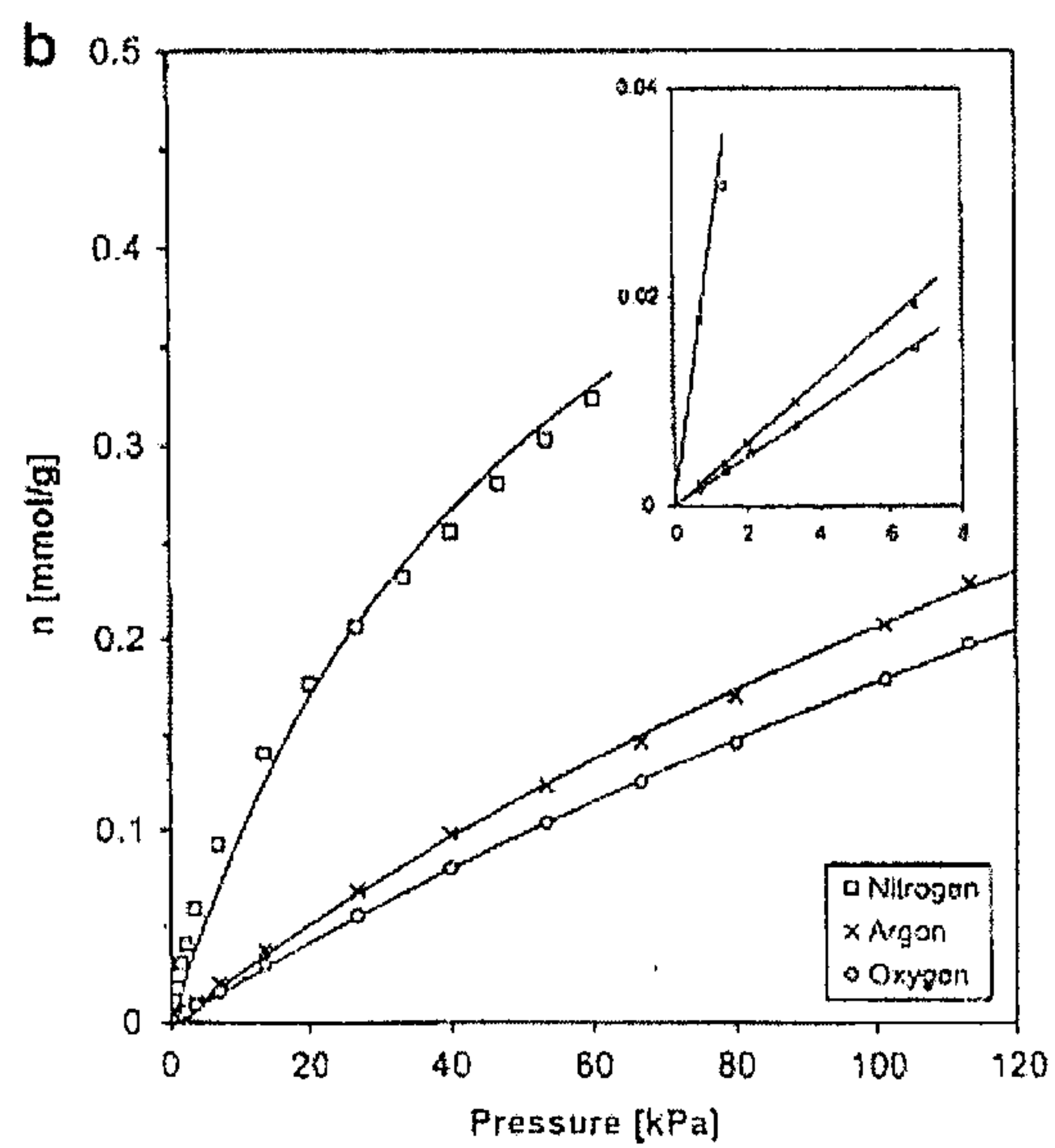


Figure 6b





20 nm